A Low-Cost Preparation of Si@C Composite Anode from Si Photovoltaic Waste

Shiyun Zhang[1], Jian Xie[1,2,*], Chunyang Wu[3], XinbingZhao[1,2]

[1] State Key Laboratory of Silicon Materials, School of Materials Science and Engineering, Zhejiang University, Hangzhou 310027, P. R. China
[2] Key Laboratory of Advanced Materials and Applications for Batteries of Zhejiang Province, Hangzhou 310027, P. R. China
[3] State Key Laboratory of Electronic Thin Films and Integrated Devices, University of Electronic Science and Technology of China, Chengdu 610054, P. R. China
[*]E-mail: xiejian1977@zju.edu.cn

Silicon materials are recognized as one of the most attractive anode materials in Li-ion batteries (LIBs) due to their ultrahigh capacity. However, there are still challenges to fabricate silicon-based anodes with a sustainable, scalable and cost-effective method. In this work, nanoscale Si was synthesized using the wafer slicing wastes from photovoltaic (PV) industry via a scalable and facile fabrication approach. After purification and sand milling, the obtained Si of 100–200 nm delivers a high discharge capacity of 2554 mAh g^{-1}. To address the potential application of the nanoscale Si in practical LIBs, a silicon/carbon composite (Si@C-G) was made, which is composed of the nanoscale Si, artificial graphite, graphene and pyrolytic carbon. The Si@C-G composite anode could yield a stable capacity of around 400 mAh g^{-1}, and a high retention rate of 91% can be achieved after 100 cycles, where the introduced graphene provide a better conducting/buffering network. Our work shows the waste Si from PV industry can be recycled and reused in LIBs industry.

1. INTRODUCTION

Li-ion batteries (LIBs) have currently become the prevailing energy storage tools and are widely used in such fields as portable electronics and electric vehicles [1–5]. With ever increasing demand in these fields, it is very urgent to make high-energy density LIBs [5, 6]. Silicon is currently regarded as the most attractive alternative to replace graphite anode in commercial LIBs, because it has ten times higher capacity (theoretically 4200 mAh g^{-1}) than graphite (theoretically 372 mAh g^{-1}) [7–12]. Besides, Si has a low working potential and, in the earth's crust, silicon is the second richest

element [7–12]. However, Si anode undergoes huge volume expansion/contraction upon lithiation/delithiation process, which results in pulverization of the electrode materials, electrical isolation between current collector and electrode material, cracking of the solid electrolyte interface (SEI) film, and thereby drastic capacity fade upon cycling [7–12]. Many methods have been adopted to deal with these issues, such as building nanostructured Si materials and composites [13–18], using new electrolyte systems [19–21] and developing novel binders [22, 23], among which, the using of nanostructured Si is found to be quite useful to enhance cycling stability of Si-based electrodes. Till now, various approaches have been adopted to synthesize nanosized silicon, e.g., chemical vapor deposition (CVD) [24, 25], etching of crystalline Si wafers [26, 27], and magnesiothermic reduction reaction of SiO_2 [28, 29]. Nevertheless, these fabrication methods are either costly, unsafe, environmentally unfriendly or have a low yield. For example, for CVD method, toxic silane precursor is used. Therefore, a challenge remains to synthesize nanoscale Si using a cost-effective, sustainable and scalable approach.

In the past few decades, the photovoltaic (PV) industry has made a rapid development. As one of the most critical factors in PV industry, a large amount of Si material is used for the fabrication of solar cells every year [30]. But in fact, a lager proportion of Si (about 40%) becomes slurry waste during the multiple wire-saw processes [30–33]. It is thus anticipated that when the Si sawdust can be effectively recycled and applied in LIBs, it will provide a low-cost and sustainable Si source for practical LIBs industry. Besides the economic aspect, it will also bring about tremendous social and environmental benefit.

In this paper, we will report on a facile and cost-effective route to synthesize nanostructured silicon-based anodes for LIBs using the PV wafer slicing wastes. Purified micrometer size Si can be obtained by acid rinsing and heat treatment of the raw Si waste. The nanoscale Si of 100–200 nm can be rapidly produced by simple sand milling method with a scalable process. The obtained nano Si gives a large first discharge capacity of 2554 mAh g^{-1}. To show a potential application of the nano Si in LIBs, a silicon/carbon composite (Si@C) was fabricated using nano Si and artificial graphite (AG) as the starting materials with coated pyrolytic carbon incorporated, which exhibits a practical capacity of ~500 mAh g^{-1}. With graphene (G) introduced, the Si@C-G composite demonstrates enhanced cycling stability (91% capacity retained after 100 cycles) due to the conducting/buffering networks constructed by graphene. This work provides a promising method to realize cost-effective, sustainable, and scalable production of nano Si by recycling the waste Si in PV industry to reuse it in LIBs industry.

2. EXPERIMENTS

2.1. Synthesis of nanoscale Si from the waste Si powder

The raw Si waste was first rinsed by stirring in a 0.1 mol L^{-1} HCl solution overnight to remove the impurity. After filtrating and drying, the obtained Si powder was put in an Al_2O_3 porcelain boat and fired at 800°C for 5 h in a tubular furnace in Ar flow to purify Si. Then, the purified Si was

dispersed into ethanol with stirring for 30 min to get a slurry followed by sand milling for 2 h using 0.3 mm ZrO_2 beads at the speed of 2300 rpm to prepare nanoscale Si.

2.2 Preparation of Si@C composite and Si@C-G composite

Si@C composite was synthesized by a facile method including processes of ball milling and spray drying. Briefly, the obtained nanoscale Si was mixed with AG (Jiangxi Zichen Technology Co., Ltd) (Si:AG = 1:7, in weight ratio) via dry ball milling for 10 h at 350 rpm to get a Si/AG mixture. Then, the Si/AG, glucose and polyvinylpyrrolidone (PVP) (Si/AG:glucose:PVP = 8:2:1, in weight) were mixed in deionized water. The above mixture was uniformly dispersed by wet ball milling for 3 h at 350 rpm. The ball-milled slurry was then spray dried to prepare the precursor of the Si@C composite with an inlet temperature of $230^{\circ}C$ and an outlet temperature of $110^{\circ}C$. Finally, the collected precursor was put in an Al_2O_3 boat and fired at $600^{\circ}C$ for 3 h in the tubular furnace in Ar flow to get the Si@C. The Si@C-G was prepared by a similar route as the Si@C composite except that commercial graphene (Changzhou the Sixth Element Materials Technology Co., Ltd) was added in the dry ball milling step (Si:AG:graphene = 1:7:0.25, in weight).

2.3 Materials characterization

The obtained materials were characterized using X-ray diffraction (XRD, X-pert Powder, PANalytical B.V.) with a Cu K_{α} radiation (λ = 0.1542 nm). Morphologies of the synthesized materials were characterized via a scanning electron microscope (SEM, SU8010, Hitachi). Thermogravimetric analysis (TGA) was performed on a DSCQ1000 instrument from 50 to $1000^{\circ}C$ with a ramping rate of $10^{\circ}C$ min^{-1} in air. Raman spectra were obtained on a Raman micro spectrometer (LabRamHRUV, JDbin-yvon) using Ar-ion laser with wavelength of 514.5 nm at 10 mW. Transmission electron microscopy (TEM) observations together with high-angle annular dark field-scanning transmission electron microscopy (HAADF-STEM) characterizations were carried out on a FEI Tecnai F20 microscope operated at 200 kV with an energy-dispersive X-ray spectroscopy (EDS) system (X-Max65T, Oxford Instruments).

2.4 Electrochemical measurements

Electrochemical properties of the obtained materials were evaluated with CR2025-type coin cells made in an Ar-filled glove box. Electrode slurry was prepared with the synthesized samples as active material (80 wt%), polyacrylic acid (PAA, 10 wt%) as binder, and acetylene black as conductive agent (10 wt%) dispersed in N-methylpyrrolidone (NMP). After sufficiently mixing by magnetic stirring and ultrasonic dispersion, the slurry was coated uniformly on Cu foil and dried first at $80^{\circ}C$ for 3 h in air, and then at $60^{\circ}C$ overnight under vacuum. Lithium foils were applied as counter electrodes and Celgard 2300 films were applied as separators. The electrolyte solution was 1 M $LiPF_6$ dissolved in a mixture of ethlylene carbonate (EC), dimethyl carbonate (DMC) and ethyl methyl carbonate

(EMC)(EC:DMC:EMC = 1:1:1, by volume ratio) with 5 vol% fluoroethylene carbonate (FEC) additive. The galvanostatic charge-discharge tests were performed on a cell cycler (Neware, China) in a 0.01–1.50 V (*vs*. Li/Li$^+$) voltage window for Si@C composite and Si@C-G electrodes (0.01–2.00 V for purified Si or sand-milled nano Si electrodes). Cyclic voltammetry (CV) plots were scanned on an electrochemistry workstation (VersaSTAT3, Princeton Applied Research) over a 0.01–1.50 V (*vs*. Li/Li$^+$) potential range at 0.1 mV s^{-1}. Electrochemical impedance spectroscopy (EIS) tests were conducted by applying an alternating voltage of 5 mV amplitude over a frequency range from 100 kHz to 0.01 Hz. The above electrochemical tests were performed at 25°C.

3. RESULTS AND DISCUSSION

Fig. 1a exhibits the SEM images of the raw Si waste. Raw Si waste particles have a plate-like shape with a size of 500 nm~4 µm. The morphology and particle size of purified Si (Fig. 1b) obtained from raw Si waste after acid rinsing and heat treatment are similar to those of raw Si waste. As seen in Fig.1c, the size of the purified Si particles has been reduced to nanoscale after sand milling for 2 h. This process is industry compatible since nano Si can be rapidly produced and the process can easily be scaled up. As mentioned above, raw Si waste is generated during the multiple wire-saw process, where the diamond wire, a steel wire coated with a large number of diamond grits by resin binder, is used as the cutting tool to slice silicon [30, 34]. As a result, the obtained waste slurry is composed of the kerf Si loss which is the dominant component, polyethylene glycol (PEG, the cutting fluid), deciduous diamond, resin binder and stainless steel fragments from the diamond wire [30, 33]. Fig. 1d demonstrates the XRD of raw Si waste, purified Si and nano Si, where the five main diffraction peaks agree well with the standard diffraction peaks of Si (JCPDS No. 27-1402). Note that compared with the raw Si waste, the purified Si and nano Si exhibit reduced noisy peaks, demonstrating that the raw Si waste has been sufficiently purified after the rinsing and heat-treatment process.
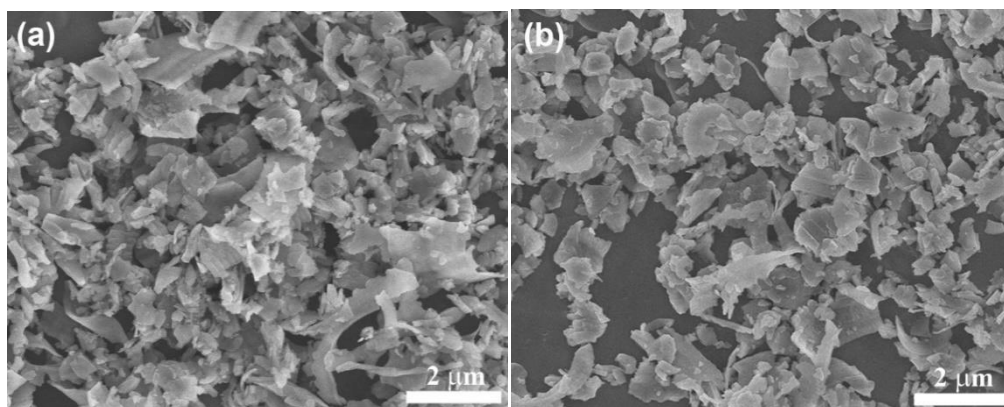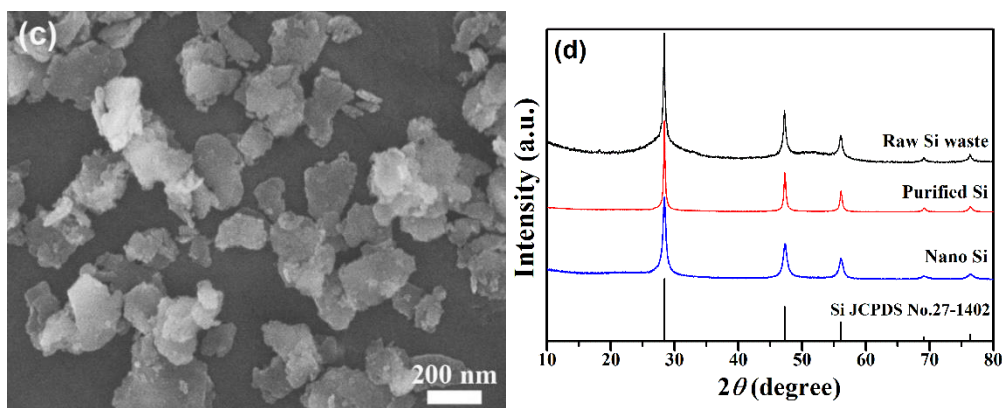
Figure 1. SEM images of (a) raw Si waste, (b) purified Si, (c) nano Si, and (d) XRD of the three samples.

Electrochemical properties of the purified Si and nano Si were investigated by galvanostatic discharge-charge cycling at 100 mA g^{-1} between 0.01 and 2.00 V. For the both materials, their discharge-charge curves (Fig. 2a, 2c) show typical lithiation/delithiation plateaus of Si at about 0.1 and 0.4 V, respectively. The curves all exhibit a sloping feature at the early stage of the first discharge, which is correlated to decomposition of electrolytes and formation of the SEI layer, and the sloping part of the curve disappears in the subsequent cycles. The purified Si electrode yields a first discharge capacity of 3049 mAh g^{-1} and a first charge capacity of 2244 mAh g^{-1}, corresponding to a first coulombic efficiency of 73.6%. However, the first discharge capacity of nano Si electrode is 2554 mAh g^{-1} with a first coulombic efficiency of 66.3%, lower than that of the purified Si electrode. That is probably because of the effect of the SiO$_x$ layer on surface of the Si particles. Nanoscale Si is more susceptible to oxidation than microsized purified Si due to higher surface activity, resulting in thicker SiO$_x$ layer on the sand-milled nano Si particles. As a result, nano Si shows a low reversible capacity and coulombic efficiency. As seen in Fig. 2b and d, nano Si shows a better cycling stability with a discharge capacity of 491 mAh g^{-1} kept after 60 cycles, while for the purified Si, the discharge capacity drops rapidly to 242 mAh g^{-1} after 60 cycles. It indicates that reducing the particle size of Si is effective to improve cycling performance for Si materials.
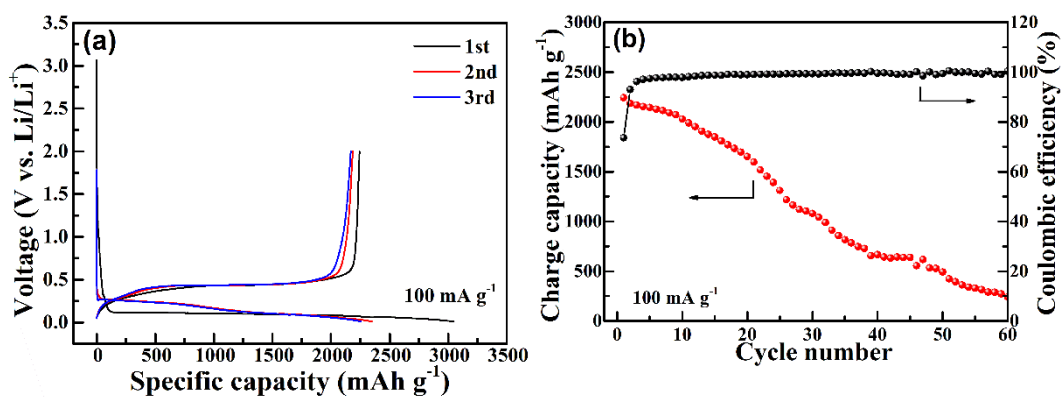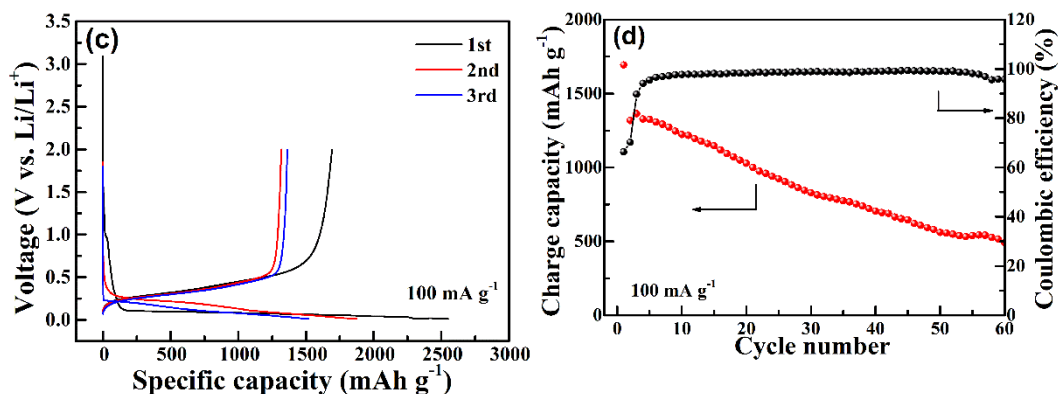
Figure 2. The first three discharge-charge curves at 100 mA g^{-1} between 0.01 and 2.00 V of (a) purified Si and (c) nano Si, and cycling performance of (b) purified Si and (d) nano Si.

To evaluate the potential application of nanoscale Si from waste Si in LIBs, Si@C and Si@C-G composites were prepared using the sand-milled purified Si as the precursors. XRD peaks of AG, Si@C and Si@C-G sample are given in Fig. 3. As expected, all diffraction peaks of Si@C and Si@C-G are consistent with those of graphite and Si, which indicates that graphite and Si were combined successfully through milling and spray drying process without introducing any impurities. To obtain the silicon content in the two composites, TGA tests were conducted as presented in Fig. 4a. According to the TGA curves, the typical combustion patterns of carbon were observed, and the weight ratio of silicon in Si@C and Si@C-G is calculated to be 14.9% and 11.5% respectively. Fig. 4b gives the Raman results of Si, Si@C and Si@C-G. The characteristic peaks at 500 and 918 cm^{-1} are in agreement with typical Raman modes of silicon, and the bands at ca. 1350 and 1580 cm^{-1} are associated with the D- and G-bands of carbon materials [17, 28, 29, 35]. The value of I_D/I_G represents the degree of graphitization, associating with the electrical conductivity of materials [35, 36]. Si@C-G presents smaller integrated intensity ratio of I_D/I_G than Si@C, meaning that Si@C-G exhibits a better electrical conductivity [35, 36].
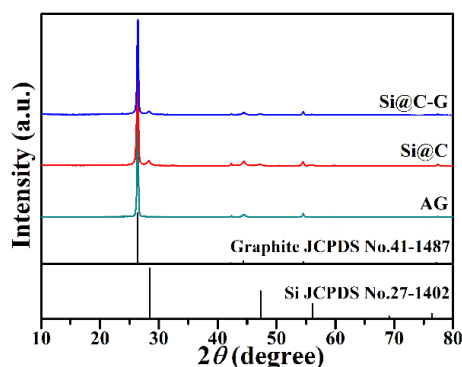
Figure 3. XRD patterns of AG, Si@C composite and Si@C-G composite.
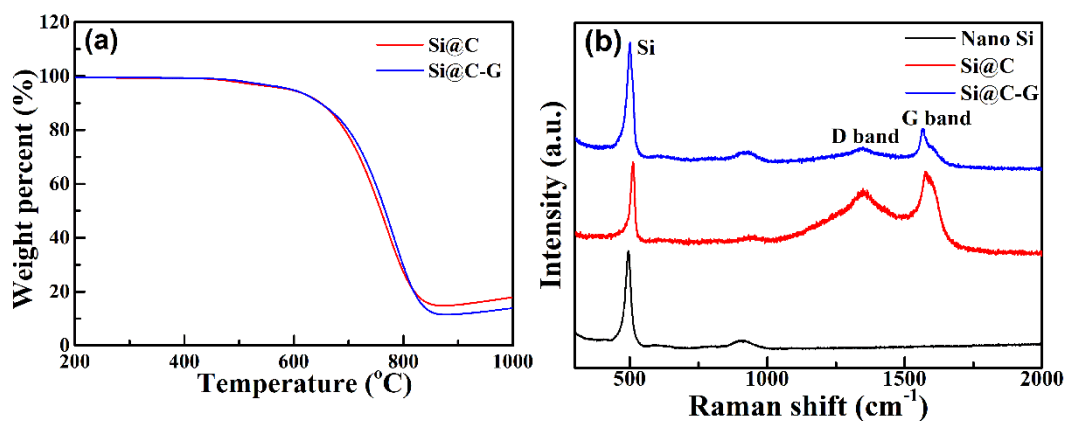
Figure 4. (a) TGA curves and (b) Raman spectra of nano Si, Si@C and Si@C-G.

The morphologies of AG, Si@C and Si@C-G composites are demonstrated in Fig. 5. Obviously, the particle size of AG is about 5–20 µm with a smooth surface (Fig. 5a, b). As presented in Fig. 5c and e, the Si@C and Si@C-G composites have a similar morphology to AG, as well as the particle size. But the surface of the both composites exhibits a rough feature with attached nanoscale Si particles (Fig. 5d, f). This indicates that the nano Si particles have been successfully loaded onto the microsized AG particles. It is expected that the pyrolytic carbon from glucose and PVP helps to stick Si nanoparticles on the surface of AG particles. The TEM and HAADF-STEM images and the corresponding EDS mapping in Fig. 6b–d also prove the presence of Si particles on the AG surfaces. As seen in Fig. 5f and 6a, graphene also covers the surface of AG in Si@C-G composite, which not only provides the conducting networks for the composite but also helps to fix the Si particles. It should be noted that compared with microszied Si, the nano Si is easier to be loaded on microsized AG to construct more uniform composite. In addition, small-sized Si also suffers alleviated volume changes and particle pulverization upon repeated cycling.
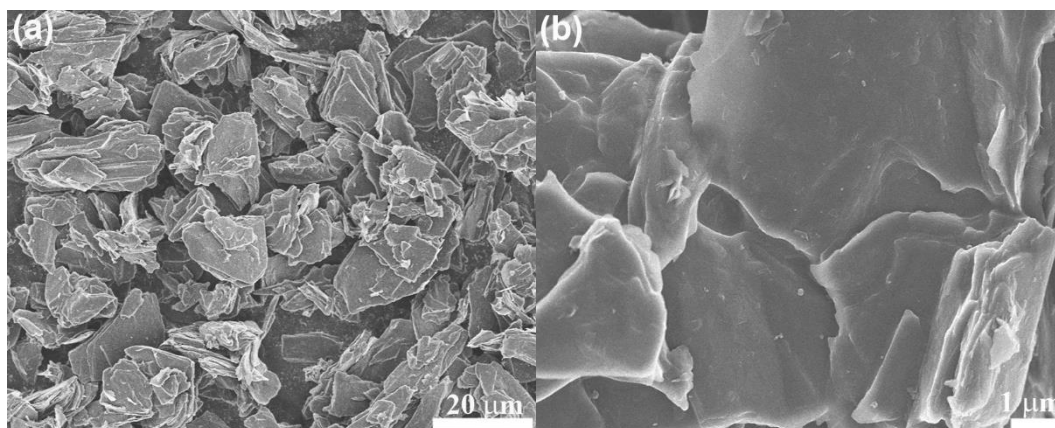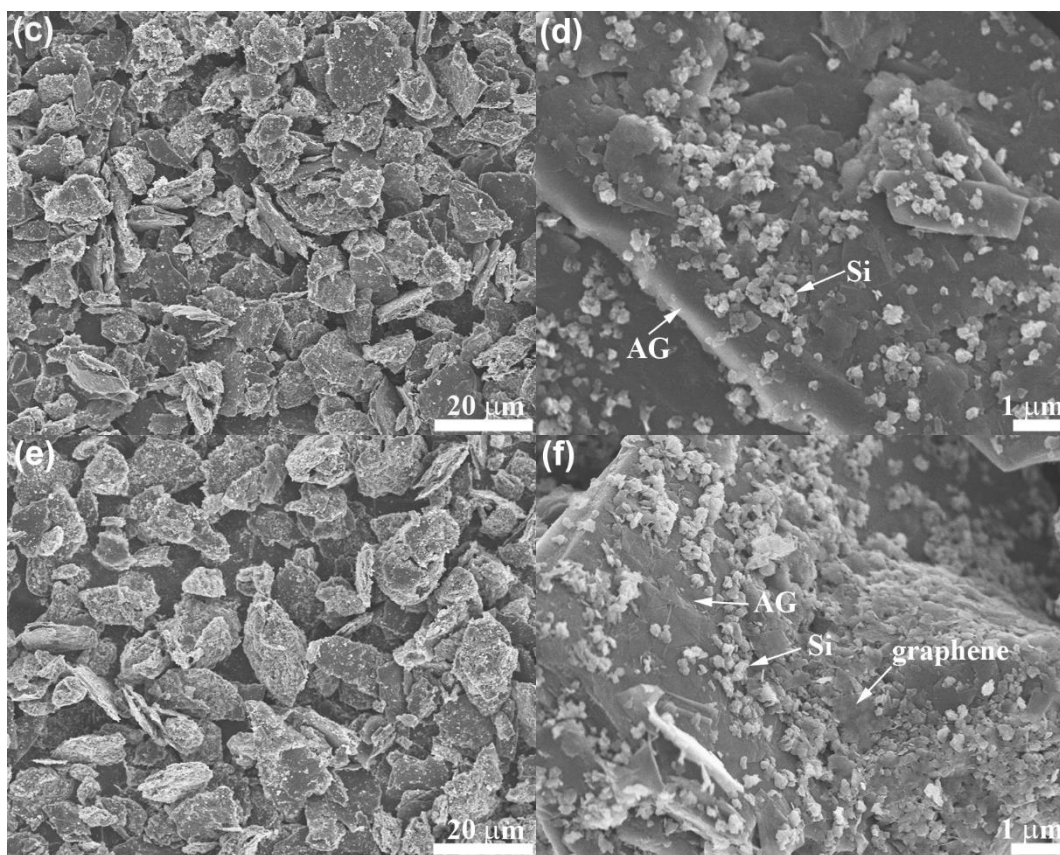
Figure 5. SEM images of (a, b) AG, (c, d) Si@C composite, and (e, f) Si@C-G composite.

To evaluate the electrochemical properties of Si@C and Si@C-G, CV, galvanostatic cycling and EIS measurements were conducted. Fig. 7 shows the CV plots performed at 0.1 mV s^{-1} in a 0.01–1.50 V potential range. For the both composites, a small/broad cathodic peak at 0.8–1.2 V could be observed in the first discharge process and it is absent in the subsequent cycles, which is associated with formation of the SEI layer [17]. The cathodic peaks (at ca. 0–0.4 V) and the anodic peaks (at ca. 0.1–0.6 V) are related to the lithiation and delithiation, respectively, of Si and graphite [17, 18, 37]. Moreover, these peaks are overlapped after the initial cycles for activation, indicating good electrochemical reversibility of Si@C and Si@C-G. Comparing with the Si@C composite, Si@C-G composite exhibits sharper peaks in CV plots, suggesting better electrochemical kinetics with graphene introduction.
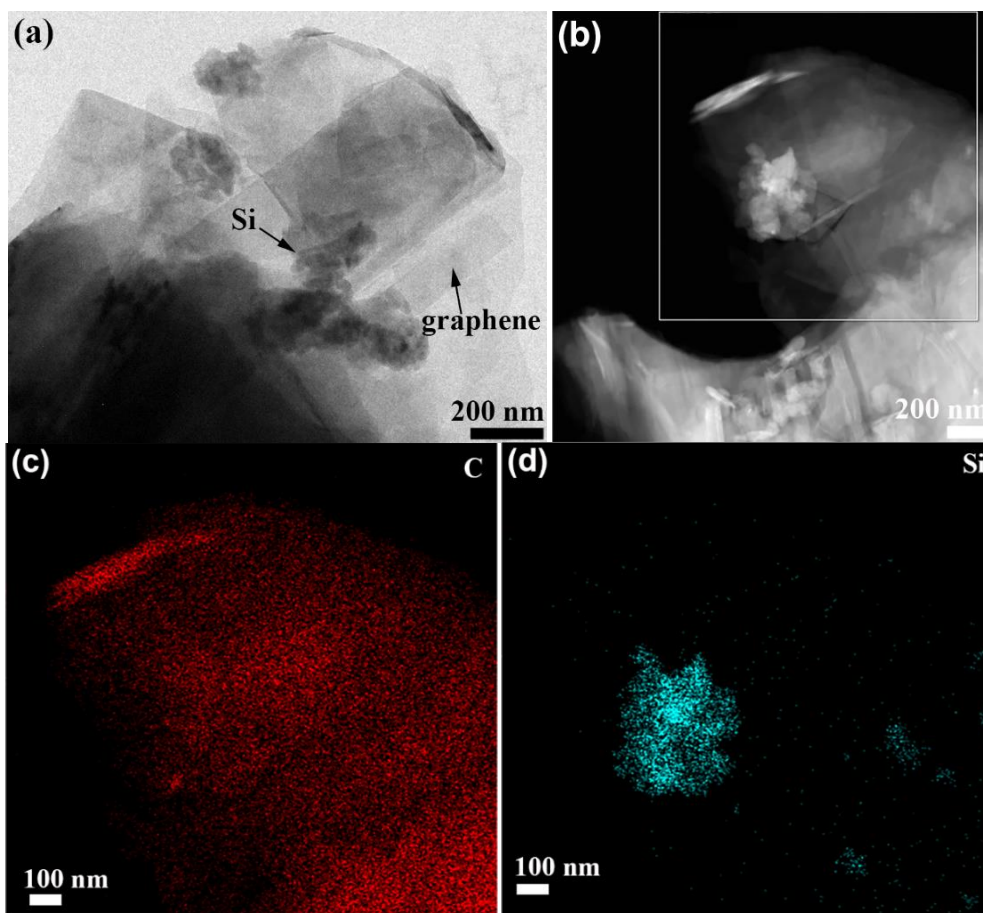
Figure 6. (a) TEM image, and (b) HAADF-STEM image and EDS mapping of (c) C and (d) Si of Si@C-G composite.

Fig. 8a and c present the first five galvanostatic discharge/charge profiles of Si@C and Si@C-G at 100 mA g^{-1} with voltage ranging from 0.01 to 1.50 V. Si@C composite delivers a first discharge capacity of 678 mAh g^{-1} and a first charge capacity of 468 mAh g^{-1}. The first discharge capacity and charge capacity of Si@C-G are 591 and 344 mAh g^{-1}, respectively. The charge capacities of both the composites gradually increase with cycling, which is probably affected by internal resistance of coin-type half-cells that show gradual activation during cycling.
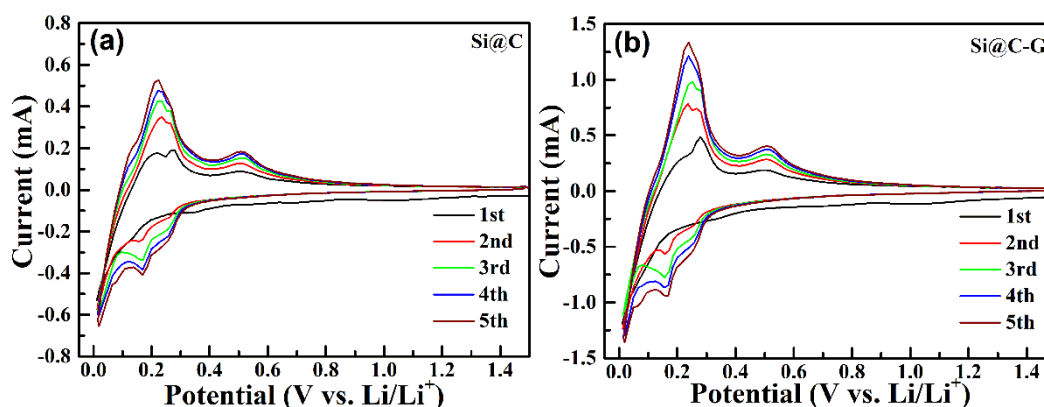
Figure 7. CV plots of (a) Si@C and (b) Si@C-G.
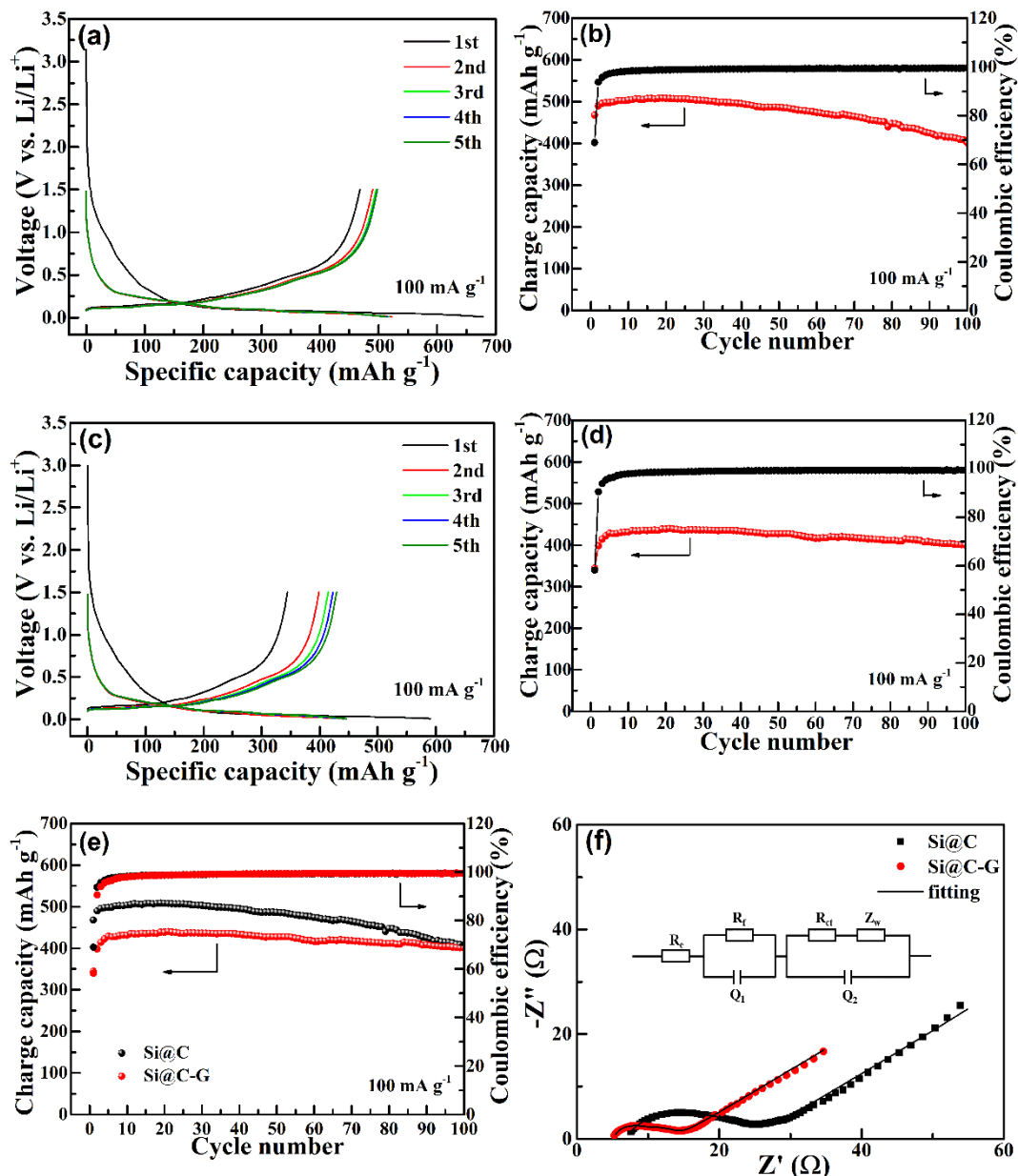
Figure 8. The first five discharge/charge profiles of (a) Si@C and (c) Si@C-G, cycling stability of (b) Si@C and (d) Si@C-G, and (e) comparison of cycling stability and (f) EIS plots after 5 cycles of Si@C and Si@C-G.

The charge capacity of Si@C reaches the highest value of 508 mAh g^{-1} in the 19th cycle and that of Si@C-G reaches the highest value of 440 mAh g^{-1} in the 21th cycle, which is consistent with the Si content from the TGA results. As expected, since the Si@C composite has a higher Si content than the Si@C-G composite, it delivers a higher capacity. However, graphene could provide a good matrix for buffering the volume changes of silicon particles and also the continuous conducting pathways for electrons during repeated cycling, which is very beneficial for electrochemical performance of the batteries. As seen in Fig. 8b and d, Si@C-G can yield a charge capacity of 401 mAh g^{-1} with the retention rate of 91% (compared with the highest value) after 100 cycles, while for

Si@C, the charge capacity decreases rapidly from the highest value of 508 to 402 mAh g^{-1} (79% retention) after 100 cycles. It should be noted that this value is higher than those of the commercial AG (360 mAh g^{-1}).

It is obvious from Fig. 8e that addition of graphene improves cycling performance of Si@C composite. To understand this, EIS measurements were performed. As shown in Fig. 8f, the Nyquist plots of the both composites are composed of a semicircle at the high-to-medium frequency area (composed of two partially overlapped semicircles), and a sloping line at the low-frequency area. The plots were fitted by an equivalent circuit (Fig. 8f) with the fitting values listed in Table 1. The two partially overlapped semicircles are related to solid electrolyte interface resistance (R_f) and charge transfer resistance (R_{ct}), respectively [38, 39]. The sloping line is related with the bulk lithium diffusion [38, 39]. With the introduction of graphene, Si@C-G composite has lower R_{ct} value than Si@C composite (Table 1).

Although bare Si can deliver a rather high theoretical capacity of 4200 mAh g^{-1}, it shoud combine with graphite and/or other carbon materials to yield a practical capacity, typically 400~600 mAh g^{-1}, due to the large volume changes of bare Si during cycling accompanied by a rapid capacity fade. Table 2 summarizes the initial capacity, cycling stability and preparation method for some Si-based anodes with a practical capacity reported so far. Note that, in the capacity range for practical applications, the cycling stability of our Si-based materials is comparale to or better than those of the previous reports at a simialr current density. It should also be adressed that the Si should be made in a facile, cost-effective method for practical applications. In this regard, our preparation method is more attractive since it uses a low-cost Si source, and the production of the Si-based materials can be realized by a scalable and sustainable route by using PV waste Si.

Table 1. Fitting results of the Nyquist plots

Sample	R_e (Ω)	R_f (Ω)	Q_1		R_{ct} (Ω)	Q_2	
			Y	n		Y	n
Si@C	7.0	10.8	$1.5×10^{-5}$	0.81	7.9	$3.9×10^{-4}$	0.69
Si@C-G	5.2	3.8	$3.8×10^{-6}$	0.97	5.0	$2.0×10^{-4}$	0.76

Table 2. Electrochamical performance comparison of Si-based anodes for LIBs

Materials	Reversible Capacity (mAh g^{-1})	Initial discharge/charge capacity (mAh g^{-1})	Current (mA g^{-1})	Silicon source	Ref.
Si/C	502.9 (50th)	887.9/624.8	100	Commercial nano-Si	[40]
Nano-Si modified graphite	442.5 (50th)	505.4/464.8	53	Nano-Si by CVD	[41]
Graphite/silicon@reGO	420.5 (50th)	771.9/575.1	50	Commercial nano-Si	[42]
SiO$_x$/C with 10wt% Si	408.5 (70th)	614.5/553.9	200	Tetraethoxysilane	[43]
Hollow Si/C composite	554 (50th)	657.9/470	100	Tetraethoxysilane	[44]

Si/SiO$_2$@C (50 wt.% C)	482 (100th)	1144.9/685.8	50	Commercial coarse SiO$_2$	[45]
Silicon/graphene/MWCNT composite	425 (100th)	2069/~1750	100	Silicon target	[46]
Si/C/NGs composite	428 (100th)	556/460.4	100	Commercial Si powders	[47]
Si/graphite@graphene	~500 (50th)	1030.3/803.3	100	Commercial Nano-Si	[48]
Si@C	402 (100th)	678/468	100	PV industry waste Si	This work
Si@C-G	401 (100th)	591/344			

4. CONCLUSIONS

In conclusion, we proposed a facile, scalable and cost-effective route to synthesize Si-based anodes for LIBs from the wafer slicing wastes. Raw Si waste was purified after facile acid rinsing and heat-treatment process, and the particle size of pure Si could be rapidly decreased to nanoscale using sand-milling method with an outstanding industrial compatibility. The nanostructured Si particles could be loaded onto AG by a facile route composed of ball milling, spray drying and high-temperature pyrolysis steps to form a uniform Si@C. The introduction of graphene in the Si@C composite provides a better conducting network and a better buffer matrix to enhance the electrochemical properties. The Si@C-G delivers a practical specific capacity of around 400 mAh g^{-1} and shows good cycle life with 91% retention after 100 cycles. Turning wastes from PV industry into valuable materials in energy applications, which not only provides a low-cost Si source to promote commercial LIBs applications of Si anodes, but realizes the recycling and reuse of waste from PV and even semiconductor industries, which kills two birds with one stone.

References

1. M. Armand and J.M. Tarascon, *Nature*, 451 (2008) 652.
2. J.B. Goodenough and Y. Kim, *Chem. Mater.*, 22 (2010) 587.
3. B. Dunn, H. Kamath and J.M. Tarascon, *Science*, 334 (2011) 928.
4. J.B. Goodenough, *Energy Storage Mater.*, 1 (2015) 158.
5. S. Chu, Y. Cui and N. Liu, *Nat. Mater.*, 16 (2016) 16.
6. J.W. Choi and D. Aurbach, *Nat. Rev. Mater.*, 1 (2016) 16013.
7. H. Wu and Y. Cui, *Nano Today*, 7 (2012) 414.
8. X. Su, Q.L. Wu, J.C. Li, X.C. Xiao, A. Lott, W.Q. Lu, B.W. Sheldon and J. Wu, *Adv. Energy Mater.*, 4 (2014) 1300882.
9. M.A. Rahman, G.S. Song, A.I. Bhatt, Y.C. Wong and C. Wen, *Adv. Funct. Mater.*, 26 (2016) 647.
10. W. Luo, X.Q. Chen, Y. Xia, M. Chen, L.J. Wang, Q.Q. Wang, W. Li and J.P. Yang, *Adv. Energy Mater.*, 7 (2017) 1701083.

11. Y. Jin, B. Zhu, Z.D. Lu, N. Liu and J. Zhu, *Adv. Energy Mater.*, 7 (2017) 1700715.
12. K. Feng, M. Li, W.W. Liu, A.G. Kashkooli, X.C. Xiao, M. Cai and Z.W. Chen, *Small*, 14 (2018) 1702737.
13. C.K. Chan, H.L. Peng, G. Liu, K. Mcilwrath, X.F. Zhang, R.A. Huggins and Y. Cui, *Nat. Nanotechnol.*, 3 (2008) 31.
14. M.H. Park, M.G. Kim, J. Joo, K. Kim, J. Kim, S. Ahn, Y. Cui and J. Cho, *Nano Lett.*, 9 (2009) 3844.
15. D. Shao, D.P. Tang, Y.J. Mai and L.Z. Zhang, *J. Mater. Chem. A*, 1 (2013) 15068.
16. Q. Xu, J.Y. Li, J.K. Sun, Y.X. Yin, L.J. Wan and Y.G. Guo, *Adv. Energy Mater.*, 7 (2017) 1601481.
17. H. Wang, J. Xie, S.C. Zhang, G.S. Cao and X.B. Zhao, *RSC Adv.*, 6 (2016) 69882.
18. G. Fang, X.L. Deng, J.Z. Zou and X.R. Zeng, *Int. J. Electrochem. Sci.*, 14 (2019) 1580.
19. Y.M. Lin, K.C. Klavetter, P.R. Abel, N.C. Davy, J.L. Snider, A. Heller and C.B. Mullins, *Chem. Commun.*, 48 (2012) 7268.
20. S.J. Lee, J.G. Han, Y. Lee, M.H. Jeong, W.C. Shin, M. Ue and N.S. Choi, *Electrochim. Acta*, 137 (2014) 1.
21. K. Schroder, J. Alvarado, T.A. Yersak, J.C. Li, N. Dudney, L.J. Webb, Y.S. Meng and K.J. Stevenson, *Chem. Mater.*, 27 (2015) 5531.
22. B. Koo, H. Kim, Y. Cho, K.T. Lee, N.S. Choi and J. Cho, *Angew. Chem. Int. Ed.*, 51 (2012) 8762.
23. Y.K. Jeong, T.W. Kwon, I. Lee, T.S. Kim, A. Coskun and J.W. Choi, *Nano Lett.*, 14 (2014) 864.
24. W. Wang and P.N. Kumta, *ACS Nano*, 4 (2010) 2233.
25. M.Y. Ge, J.P. Rong, X. Fang and C.W. Zhou, *Nano Lett.*, 12 (2012) 2318.
26. B.M. Bang, H. Kim, H.K. Song, J. Cho and S. Park, *Energy Environ. Sci.*, 4 (2011) 5013.
27. A. Vlad, A.L.M. Reddy, A. Ajayan, N. Singh, J.F. Gohy, S. Melinte and P.M. Ajayan, *Proc. Natl. Acad. Sci.USA*, 109 (2012) 15168.
28. H. Wu, N. Du, X.X. Shi and D.Y. Yang, *J. Power Sources*, 331 (2016) 76.
29. Y.C. Ru, D.G. Evans, H. Zhu and W.S. Yang, *RSC Adv.*, 4 (2014) 71.
30. L.Y. Zhang, L. Zhang, J. Zhang, W.W. Hao and H.H. Zheng, *J. Mater. Chem. A*, 3 (2015) 15432.
31. T.Y. Wang, Y.C. Lin, C.Y. Tai, C.C. Fei, M.Y. Tseng and C.W. Lan, *Prog. Photovolt: Res. Appl.*, 17 (2009) 155.
32. T.Y. Wang, Y.C. Lin, C.Y. Tai, R. Sivakumar, D.K. Rai and C.W. Lan, *J. Cryst. Growth*, 310 (2008) 3403.
33. H.D. Jang, H. Kim, H. Chang, J. Kim, K.M. Roh, J.H. Choi, B.G. Cho, E. Park, H. Kim, J.Y. Luo and J.X. Huang, *Sci. Rep.*, 5 (2015) 9431.
34. C.H. Chuang and L.V. Nhat, *Int. J. Precis. Eng. Man.*, 15 (2014) 789.
35. Q. Xu, J.K. Sun, J.Y. Li, Y.X. Yin and Y.G. Guo, *Energy Storage Mater.*, 12 (2018) 54.
36. Q. Xu, J.K. Sun, Y.X. Yin and Y.G. Guo, *Adv. Funct. Mater.*, 28 (2018) 1705235.
37. G. Li, J.Y. Li, F.S. Yue, Q. Xu, T.T. Zuo,Y.X. Yin and Y.G. Guo, *Nano Energy*, 60 (2019) 485.
38. J.Y. Li, G. Li, J. Zhang, Y.X. Yin, F.S. Yue, Q. Xu and Y.G. Guo, *ACS Appl. Mater. Interfaces*, 11 (2019) 4057.
39. C. Liu, Z.Q. Gu, Z. Zhou, Y.X. Chen, Y.D. He, X.H. Xia and H.B. Liu, *Int. J. Electrochem. Sci.*, 14 (2019)5331.
40. M.R. Su, Z.X. Wang, H.J. Guo, X.H. Li, S.L. Huang, L. Gan and W. Xiao, *Powder Technol.*, 249 (2013) 105.
41. J. Hou, B.L. Gong, C.P. Hou, B.P. Wang, D. Yang and X.W. Wang. *Int. J. Electrochem. Sci.*, 14 (2019) 3455.
42. L. Gan, H.J. Guo, Z.X. Wang, X.H. Li, W.J. Peng, J.X. Wang, S.L. Huang and M.R. Su, *Electrochim. Acta*, 104 (2013) 117.
43. H. Cui, K. Chen, Y.F. Shen and Z. Wang, *Int. J. Electrochem. Sci.*, 13 (2018) 5474.
44. H.H. Zhang, X.H. Li, H.J. Guo, Z.X. Wang and Y. Zhou, *Powder Technol.*, 299 (2016) 178.
45. Y. Zhou, Z.Y. Tian, R.J. Fan, S.R. Zhao, R. Zhou, H.J. Guo and Z.X. Wang, *Powder Technol.*, 284

(2015) 365.

46. U. Tocoğlu, G. Hatipoğlu, M. Alaf, F. Kayış and H. Akbulut, *Appl. Surf. Sci.*, 389 (2016) 507.
47. Z.L. Wang, Z.M. Mao, L.F. Lai, M. Okubo, Y.H. Song, Y.J. Zhou, X. Liu and W. Huang, *Chem. Eng. J.*, 313 (2017) 187.
48. M.R. Su, Z.X. Wang, H.J. Guo, X.H. Li, S.L. Huang, W. Xiao and L. Gan, *Electrochim. Acta*, 116 (2014) 230.